Stanford Exploration Project, Report SERGEY, May 1, 2000, pages 583–595

Velocity continuation in migration velocity analysis

Sergey Fomel[1]

ABSTRACT

Velocity continuation can be applied to migration velocity analysis. It enhances residual NMO correction by properly taking into account both vertical and lateral movements of reflectors caused by the change in migration velocity. I exemplify this fact with simple data tests.

INTRODUCTION

Migration velocity analysis is a routine part of prestack time migration applications. It serves both as a tool for velocity estimation (Deregowski, 1990) and as a tool for optimal stacking of migrated seismic sections and modeling zero-offset data for depth migration (Kim et al., 1997). In the most common form, migration velocity analysis amounts to residual moveout correction on CRP (common reflection point) gathers. However, in the case of dipping reflectors, this correction does not provide optimal focusing of reflection energy, since it does not account for lateral movement of reflectors caused by the change in migration velocity. In other words, different points on a stacking hyperbola in a CRP gather can correspond to different reflection points at the actual reflector. The situation is similar to that of the conventional NMO velocity analysis, where the reflection point dispersal problem is usually overcome with the help of DMO (Deregowski, 1986; Hale, 1991). An analogous correction is required for optimal focusing in the post-migration domain. In this paper, I propose and test velocity continuation as a method of migration velocity analysis. The method enhances the conventional residual moveout correction by taking into account lateral movements of migrated reflection events.

Velocity continuation is an artificial process of transforming time migrated images according to the changes in migration velocity. This process has wave-like properties, which have been described in my earlier papers (Fomel, 1994, 1996, 1997). Hubral et al. (1996) and Schleicher et al. (1997) use the term *image waves* to introduce a similar concept. Velocity continuation extends the theory of residual and cascaded migrations (Rothman et al., 1985; Larner and Beasley, 1987). In practice, the continuation process can be modeled by finite-difference or spectral methods (Fomel and Claerbout, 1997; Fomel, 1998).

Applying velocity continuation to migration velocity analysis involves the following steps:

[1]**email:** sergey@sep.stanford.edu

1. prestack common-offset (and common-azimuth) migration - to generate the initial data for continuation,

2. velocity continuation with stacking across different offsets - to transform the offset data dimension into the velocity dimension,

3. picking the optimal velocity and slicing through the migrated data volume - to generate an optimally focused image.

In this paper, I demonstrate all three steps, using a simple two-dimensional dataset. For the implementation of velocity continuation, I chose the Fourier spectral method. The method has its limitations (Fomel, 1998), but looks optimal in terms of the accuracy versus efficiency tradeoff. It is important to note that although the velocity continuation result could be achieved in principle by using prestack residual migration in Kirchhoff (Etgen, 1990) or Stolt (Stolt, 1996) formulation, the first is evidently inferior in efficiency, and the second is not convenient for velocity analysis across different offsets, because it mixes them in the Fourier domain (Sava, 1999).

PUTTING TOGETHER PRESTACK VELOCITY CONTINUATION

Velocity continuation in the zero-offset (post-stack case) can be performed with a simple Fourier-domain algorithm (Fomel, 1998):

1. Input an image, migrated with velocity v_0.

2. Transform the time axis t to the squared time coordinate: $\sigma = t^2$.

3. Apply a fast Fourier transform (FFT) on both the squared time and the midpoint axis. The squared time σ transforms to the frequency Ω, and the midpoint coordinate x transforms to the wavenumber k. We can safely assume that in the post-migration domain seismic images are uniformly sampled in x, which allows us to use the FFT technique. In the case of 3-D data, FFT should be applied in both midpoint coordinates.

4. Apply a phase-shift operator to transform to different velocities v:

$$\hat{P}(\Omega,k,v) = \hat{P}_0(\Omega,k)\, e^{\frac{ik^2\left(v_0^2-v^2\right)}{4\Omega}} . \tag{1}$$

5. Apply an inverse FFT to transform from Ω and k to σ and x.

6. Apply an inverse time stretch to transform from σ to t.

The computational complexity of this algorithm has the same order as that of the Stolt migration (Stolt, 1978), but in practice it can be even faster because of the very simple inner computation.

To generalize algorithm (1) to the prestack case, we first need to include the residual NMO term (Fomel, 1996). Residual normal moveout can be formulated with the help of the differential equation:

$$\frac{\partial P}{\partial v} + \frac{h^2}{v^3 t}\frac{\partial P}{\partial t} = 0\,, \tag{2}$$

where h stands for the half-offset. The analytical solution of equation (2) has the form of the residual NMO operator:

$$P(t,h,v) = P_0\left(\sqrt{t^2 + h^2\left(\frac{1}{v_0^2} - \frac{1}{v^2}\right)}, h\right)\,. \tag{3}$$

After transforming to the squared time $\sigma = t^2$ and the corresponding Fourier frequency Ω, equation (2) takes the form of the ordinary differential equation

$$\frac{d\hat{P}}{dv} + i\Omega\frac{2h^2}{v^3}\hat{P} = 0 \tag{4}$$

with the analytical frequency-domain phase-shift solution

$$\hat{P}(\Omega,h,v) = \hat{P}_0(\Omega,h)e^{i\Omega h^2\left(\frac{1}{v_0^2}-\frac{1}{v^2}\right)}\,. \tag{5}$$

To obtain a Fourier-domain prestack velocity continuation algorithm, we just need to combine the phase-shift operators in equations (1) and (5) and to include stacking across different offsets. The algorithm takes the following form:

1. Input a set of common-offset images, migrated with velocity v_0.
2. Transform the time axis t to the squared time coordinate: $\sigma = t^2$.
3. Apply a fast Fourier transform (FFT) on both the squared time and the midpoint axis. The squared time σ transforms to the frequency Ω, and the midpoint coordinate x transforms to the wavenumber k.
4. Apply a phase-shift operator to transform to different velocities v:

$$\hat{P}(\Omega,k,v) = \sum_h \hat{P}_0(\Omega,k,h)\,e^{i\frac{k^2\left(v_0^2-v^2\right)}{4\Omega}}\,e^{i\Omega h^2\left(\frac{1}{v_0^2}-\frac{1}{v^2}\right)}\,. \tag{6}$$

   To save memory, the continuation step is immediately followed by stacking.
5. Apply an inverse FFT to transform from Ω and k to σ and x.
6. Apply an inverse time stretch to transform from σ to t.

One can design similar algorithms by using finite differences or Chebyshev spectral methods (Fomel, 1998).

The complete theory of prestack velocity continuation also requires a residual DMO operator (Etgen, 1990; Fomel, 1996, 1997). However, the difficulty of implementing this operator is not fully compensated by its contribution to the full velocity continuation. For simplicity, I decided not to include residual DMO in the current implementation.

Figure 1 shows impulse responses of prestack velocity continuation. The input for producing this figure was a time-migrated constant-offset section, corresponding to an offset of 1 km and a constant migration velocity of 1 km/s. In full accordance with the theory (Fomel, 1996), three spikes in the input section transformed into shifted ellipsoids after continuation to a higher velocity and into shifted hyperbolas after continuation to a smaller velocity.

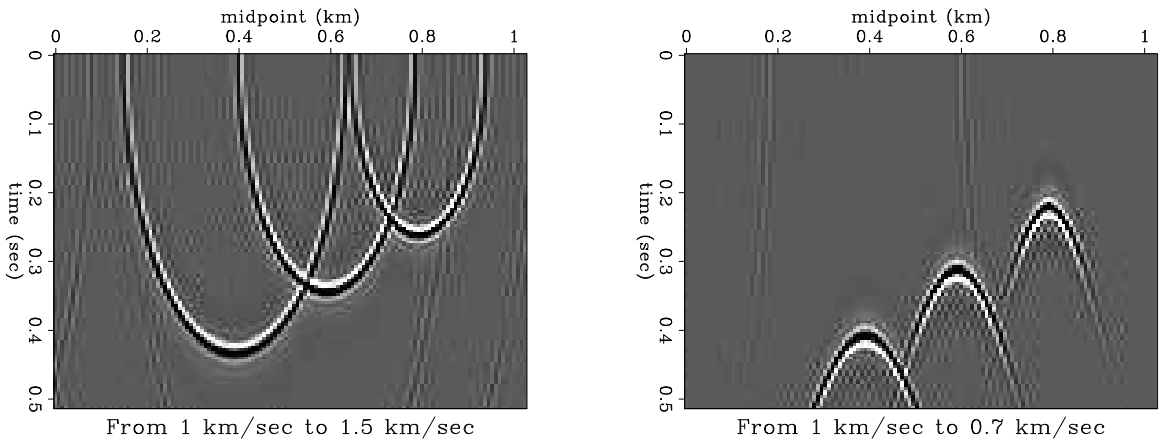

Figure 1: Impulse responses of prestack velocity continuation. Left plot: continuation from 1 km/s to 1.5 km/s. Right plot: continuation from 1 km/s to 0.7 km/s. Both plots correspond to the offset of 1 km. velmva-velimp [ER]

Figure 2 compares the result of a constant-velocity prestack migration with the velocity of 1.8 km/s, applied to the infamous Gulf of Mexico dataset from *Basic Earth Imaging* (Claerbout, 1995) and the result of velocity continuation to the same velocity from a migration with a smaller velocity of 1.3 km/s. The differences in the top part of the images are explained by differences in muting. In the first case, muting was applied after migration, and in the second case, muting was applied prior to velocity continuation. The other parts of the sections look very similar, as expected from the theory.

Velocity continuation creates a time-midpoint-velocity cube (four-dimensional for 3-D data), which we can use for picking RMS velocities in the same way as we would use the result of common-midpoint or common-reflection-point velocity analysis. The important difference is that velocity continuation provides an optimal focusing of the reflection energy by properly taking into account both vertical and lateral movements of reflector images with changing migration velocity. Figure 3 compares velocity spectra (semblance panels) at a CRP location of about 11.5 km after residual NMO and after prestack velocity continuation. Although the overall difference between the two panels is small, the velocity continuation panel

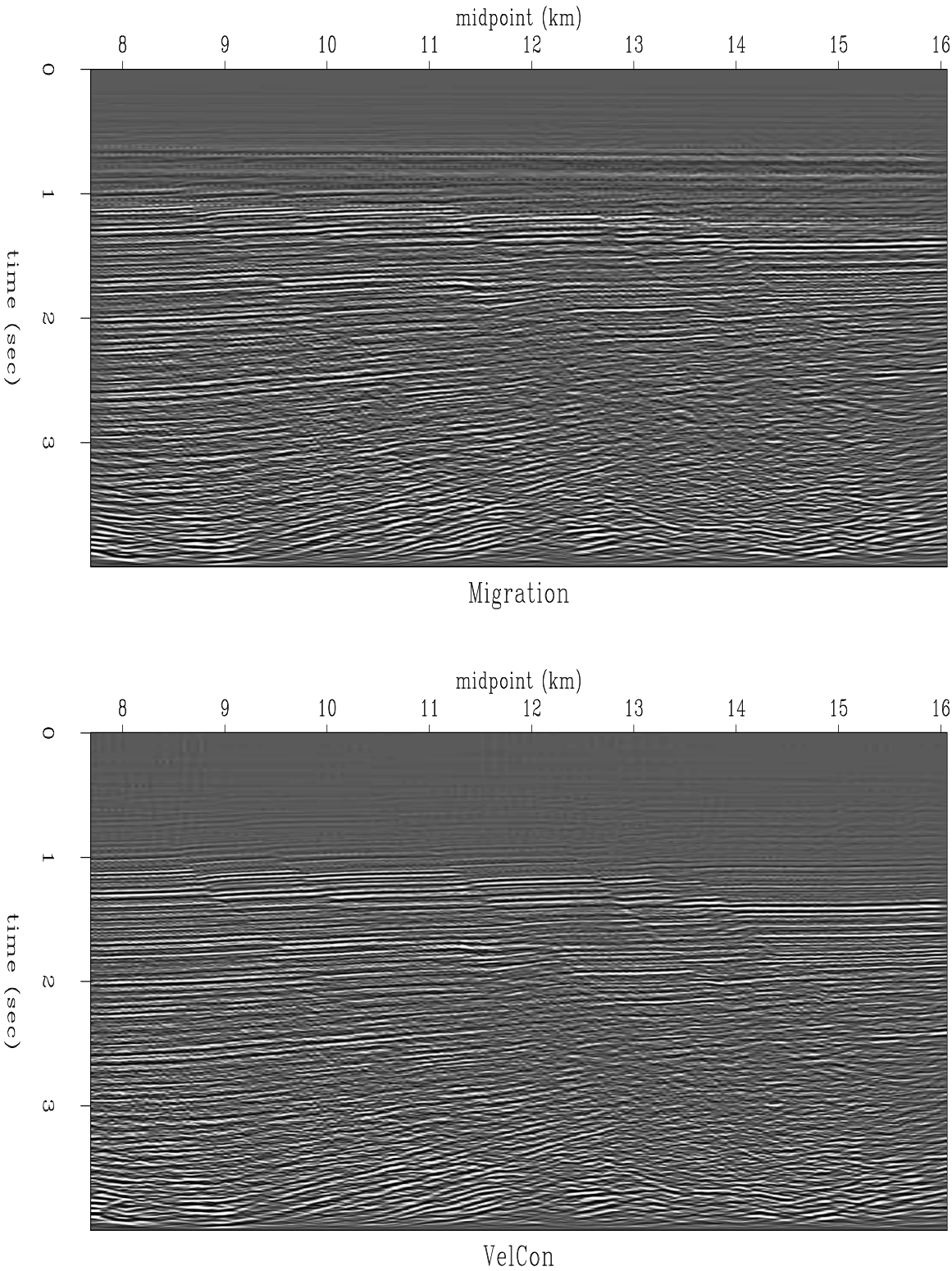

Figure 2: Top: The Gulf of Mexico dataset from *BEI* after prestack migration with the constant velocity of 1.8 km/s. Bottom: The same data after after velocity continuation from 1.3 km/s to 1.8 km/s. velmva-velmigr [ER]

shows a noticeably better focusing, especially in the region of conflicting dips between 1 and 2 seconds. The next section discusses the velocity picking step in more details.

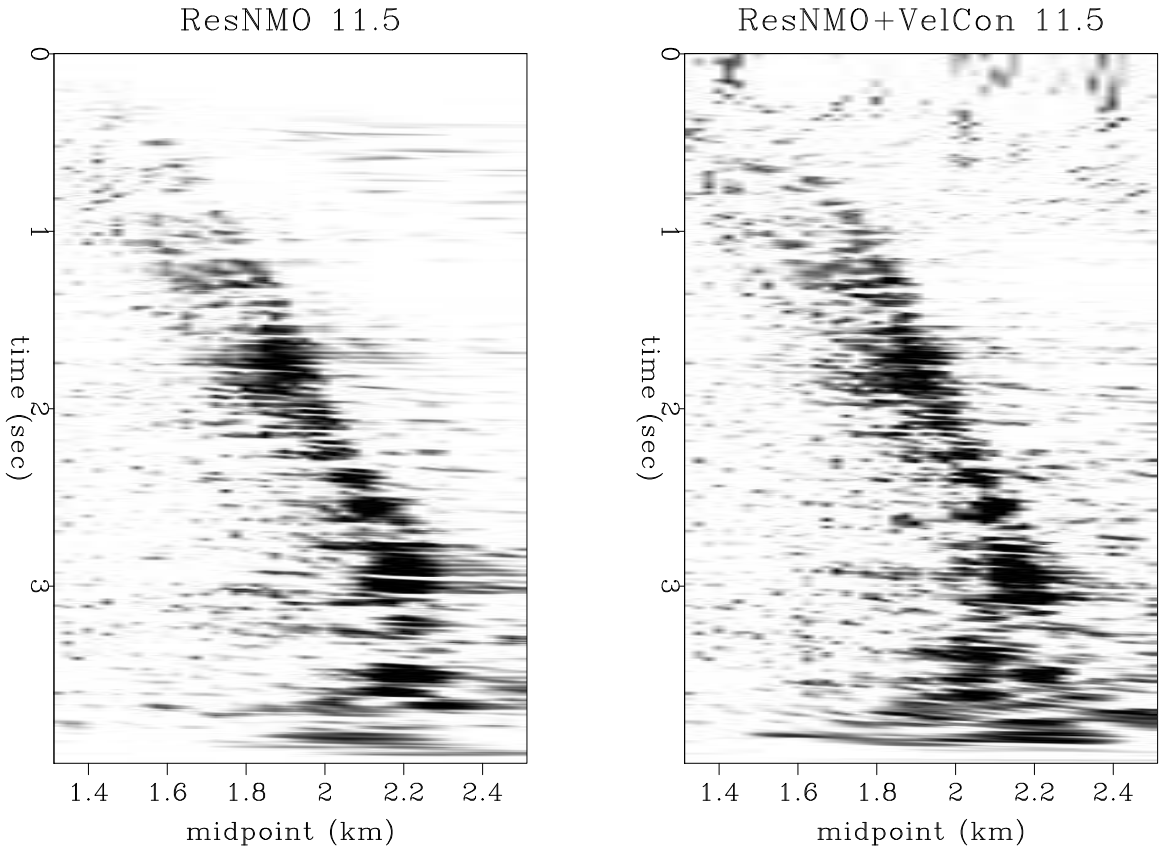

Figure 3: Velocity spectra around 11.5 km CRP after residual NMO (left) and after prestack velocity continuation (right). The right plot shows improved focusing in the region between 1 and 2 seconds. velmva-consmb [CR]

VELOCITY PICKING AND SLICING

After the velocity continuation process has created a velocity cube in the prestack common-offset migration domain, we can pick the best focusing velocity from that cube. To automatize the velocity picking procedure, I have designed a simple algorithm. The algorithm based on solving the following regularized least-square system:

$$\left\{ \begin{array}{lcl} \mathbf{W}\mathbf{x} & \approx & \mathbf{W}\mathbf{p} \\ \epsilon\mathbf{D}\mathbf{x} & \approx & \mathbf{0} \end{array} \right. . \tag{7}$$

Here $\mathbf{p}$ are blind maximum-semblance picks (possibly in a predefined fairway), $\mathbf{x}$ is the estimated velocity picks, $\mathbf{W}$ is the weighting operator with the weight corresponding to the semblance values at $\mathbf{p}$, $\mathbf{D}$ is a roughening operator, and ϵ is the scalar regularization parameter. The first least-square fitting goal in (7) states that the estimated velocity picks should match

the measured picks where the semblance is high enough[2]. The second fitting goal tries to find the smoothest velocity function possible. The least-square solution of problem (7) takes the form

$$\mathbf{x} = \left(\mathbf{W}^2 + \epsilon^2 \mathbf{D}^T \mathbf{D}\right)^{-1} \mathbf{W}^2 \mathbf{p}\,, \tag{8}$$

where $\mathbf{D}^T$ denotes the adjoint operator. In the case of picking a one-dimensional velocity function from a single semblance panel, we can simplify the algorithm by choosing $\mathbf{D}$ to be the a convolution with the derivative filter $(1, -1)$. It is easy to notice that in this case the inverted matrix in formula (8) has a tridiagonal structure and therefore can be easily inverted with a linear-time algorithm. The regularization parameter ϵ controls the amount of smoothing of the estimated velocity function. Figure 4 shows a velocity spectrum and two automatic picks for different values of ϵ.

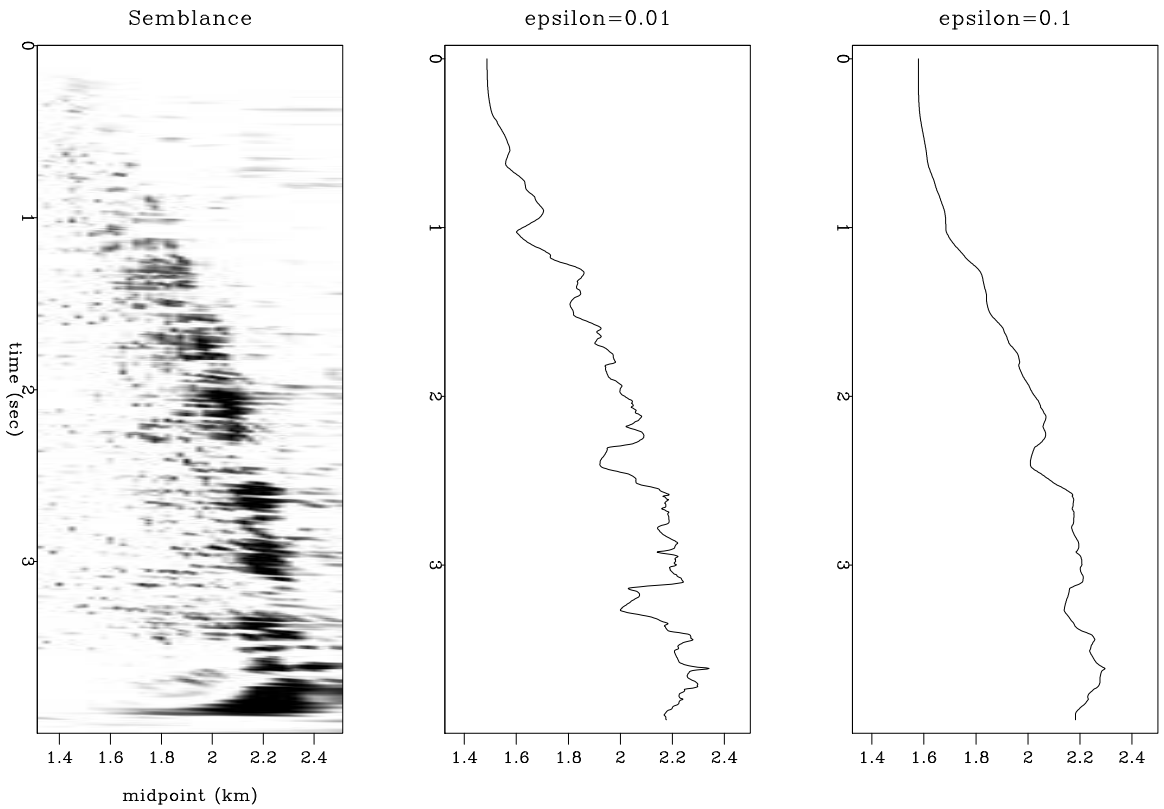

Figure 4: Semblance panel (left) and automatic velocity picks for different values of the regularization parameter. Center: $\epsilon = 0.01$, right: $\epsilon = 0.1$. Higher values of ϵ lead to smoother velocities. velmva-velpick [ER]

In the case of picking two- or three-dimensional velocity functions, one could generalize problem (7) by defining $\mathbf{D}$ as a 2-D or 3-D roughening operator. I chose to use a more

[2]Of course, this goal might be dangerous, if the original picks $\mathbf{p}$ include regular noise (such as multiple reflections) with high semblance value (Toldi, 1985). For simplicity, and to preserve the linearity of the problem, we assume that this is not the case.

simplistic approach. I transform system (7) to the form

$$\left\{ \begin{array}{rcl} \mathbf{W}\mathbf{x} & \approx & \mathbf{W}\mathbf{p} \\ \epsilon\mathbf{D}\mathbf{x} & \approx & \mathbf{0} \\ \lambda\mathbf{x} & \approx & \lambda\mathbf{x_0} \end{array} \right. , \tag{9}$$

where $\mathbf{x}$ is still one-dimensional, and $\mathbf{x}_0$ is the estimate from the previous midpoint location. The scalar parameter λ controls the amount of lateral continuity in the estimated velocity function. The least-square solution to system (9) takes the form:

$$\mathbf{x} = \left(\mathbf{W}^2 + \epsilon^2 \mathbf{D}^T \mathbf{D} + \lambda^2 \mathbf{I}\right)^{-1} \left(\mathbf{W}^2 \mathbf{p} + \lambda^2 \mathbf{x_0}\right) , \tag{10}$$

where $\mathbf{I}$ denotes the identity matrix. Formula (10) also reduces to an efficient tridiagonal matrix inversion. Figure 5 shows a result of two-dimensional velocity picking after velocity continuation. I used values of $\epsilon = 0.1$ and $\lambda = 0.1$. The first parameter controls the vertical smoothing of velocities, while the second parameter controls the amount of lateral continuity. Figure 6 shows the final result of velocity continuation: an image, obtained by slicing through

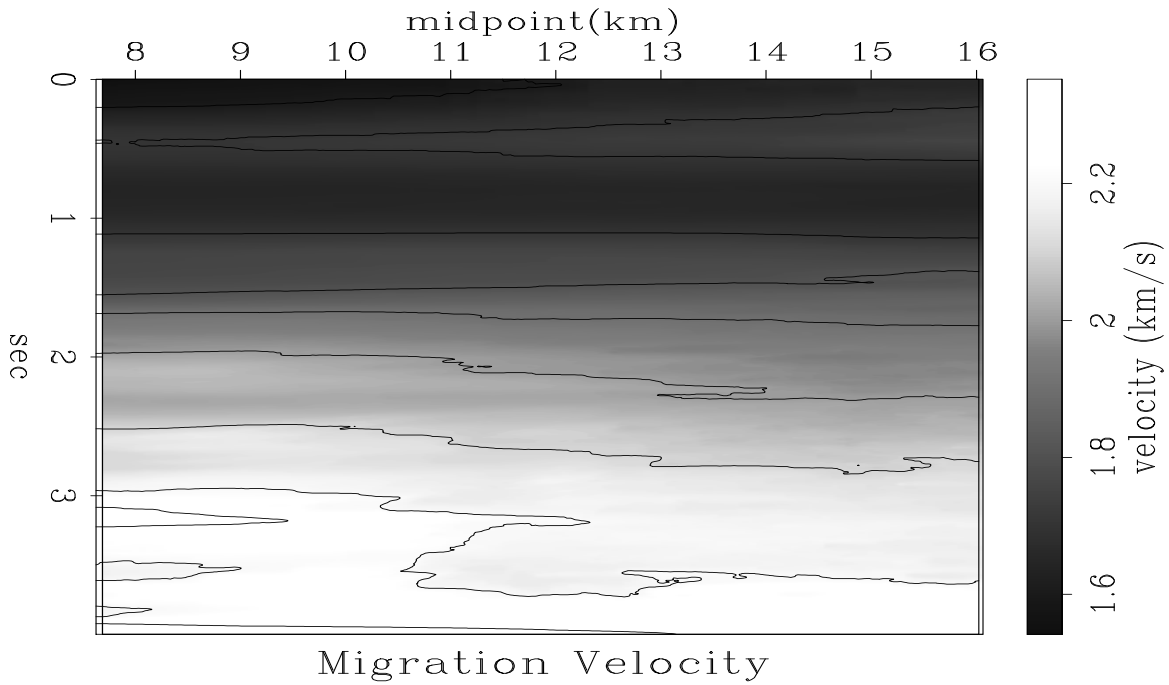

Figure 5: Automatic picks of 2-D RMS velocity after velocity continuation. The contour spacing is 0.1 km/s, starting from 1.5 km/s. velmva-beifpk [CR]

the velocity cube with the picked RMS velocity. Different parts of the image have been properly positioned and focused by the velocity continuation process. One way to further improve the image quality is *hybrid migration*: demigration to zero-offset, followed by post-stack depth migration (Kim et al., 1997). This step requires constructing an interval velocity model from the picked RMS velocities. Without repeating the details of the procedure, Figures 7 and 8 show picked RMS velocities and the velocity continuation image for the Blake Outer Ridge data, shown in many other papers in this report.

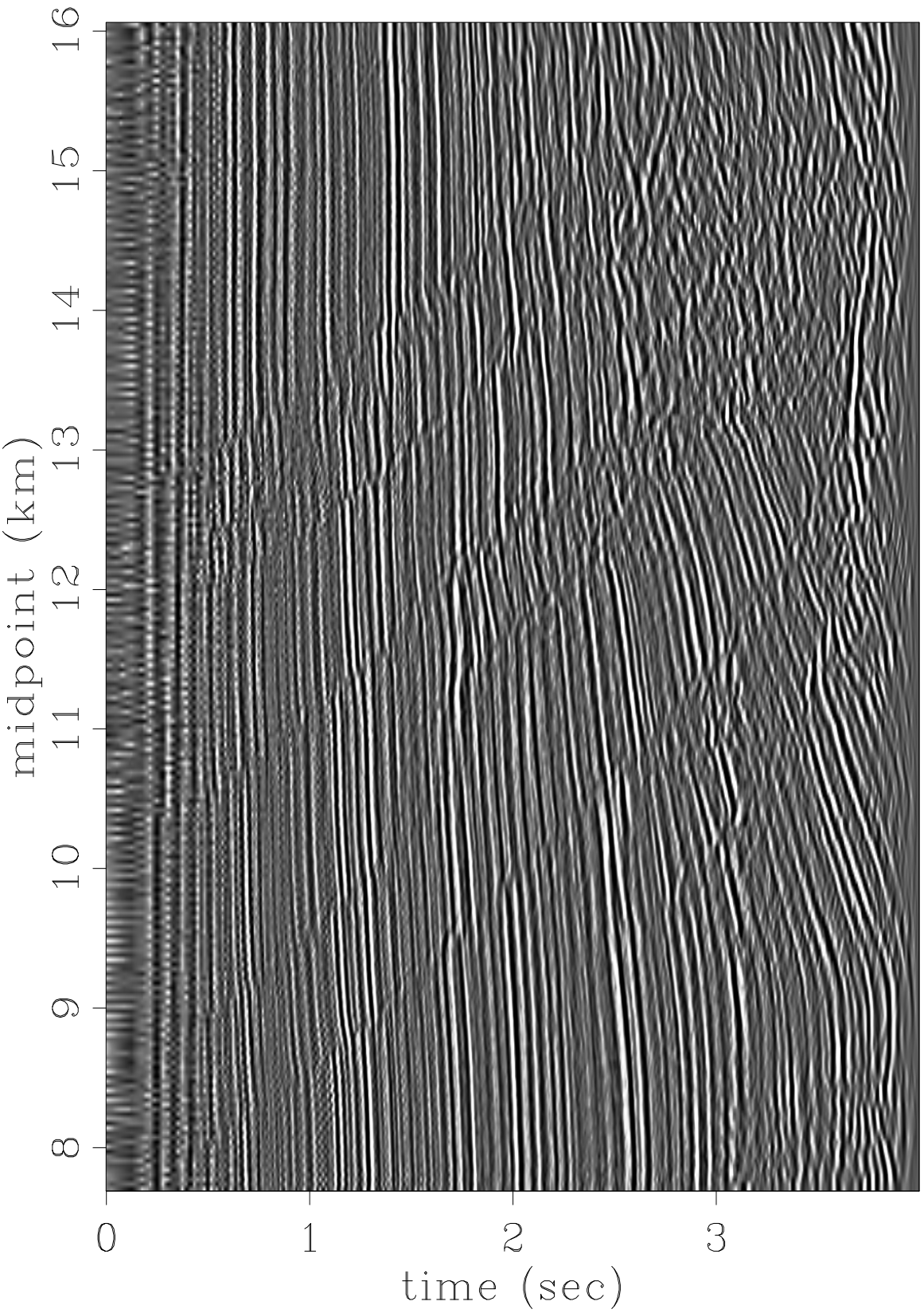

Figure 6: Final result of velocity continuation: seismic image, obtained by slicing through the velocity cube. velmva-beifmg [CR]

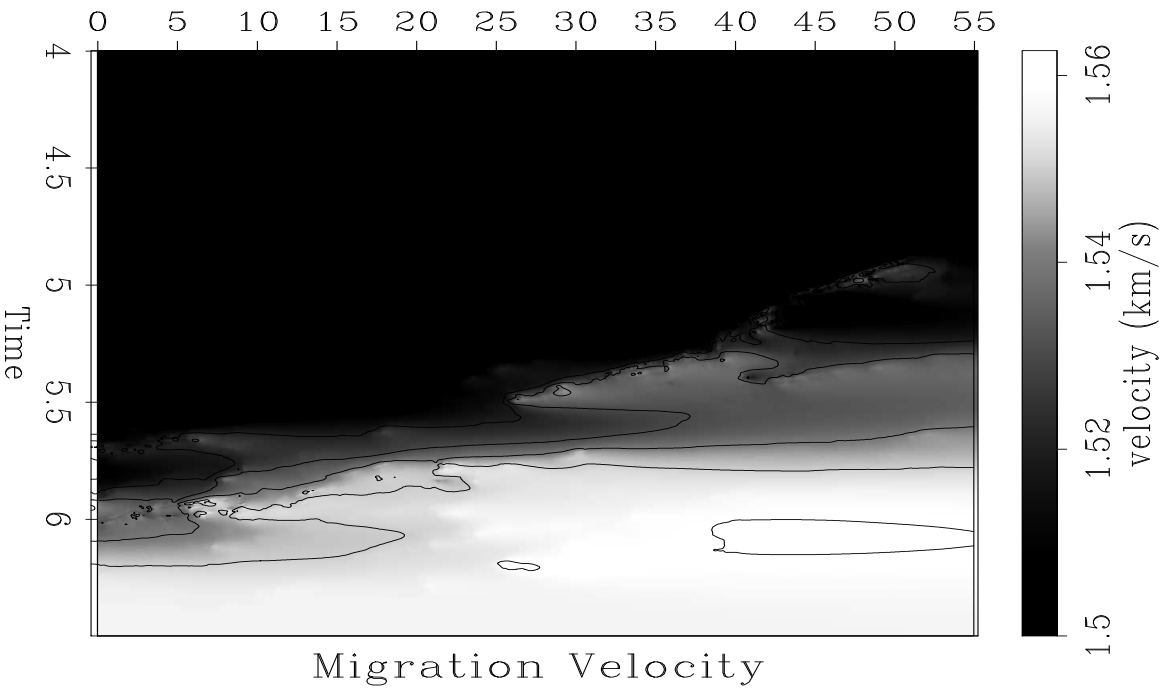

Figure 7: Blake Outer Ridge data. Automatic picks of 2-D RMS velocity after velocity continuation. The contour spacing is 0.01 km/s, starting from 1.5 km/s. velmva-pck [CR]

CONCLUSIONS

I have demonstrated an application of velocity continuation to migration velocity analysis on simple data sets. The first results look promising and encourage further real data tests, hopefully with 3-D data.

ACKNOWLEDGMENTS

I thank Jon Claerbout, Biondo Biondi, and Bill Symes for useful and stimulating discussions.

REFERENCES

Claerbout, J. F., 1995, Basic Earth Imaging: Stanford Exploration Project.

Deregowski, S. M., 1986, What is DMO: First Break, **4**, no. 7, 7–24.

Deregowski, S. M., 1990, Common-offset migrations and velocity analysis: First Break, **8**, no. 6, 224–234.

Etgen, J., 1990, Residual prestack migration and interval velocity estimation: Ph.D. thesis, Stanford University.

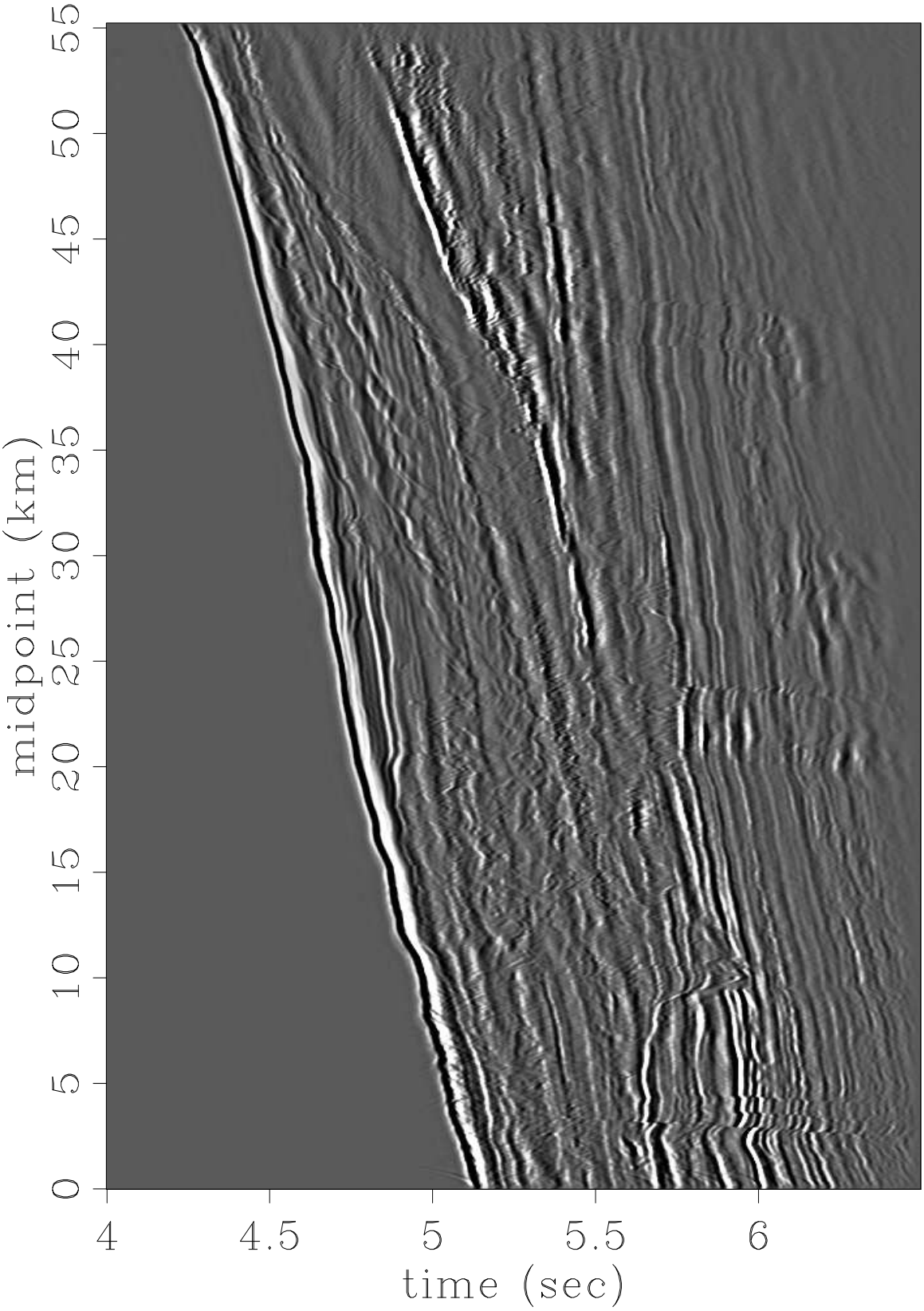

Figure 8: Blake Outer Ridge data. Final result of velocity continuation: seismic image, obtained by slicing through the velocity cube. velmva-img [CR]

Fomel, S., and Claerbout, J. F., 1997, Exploring three-dimensional implicit wavefield extrapolation with the helix transform: SEP–**95**, 43–60.

Fomel, S. B., 1994, Method of velocity continuation in the problem of temporal seismic migration: Russian Geology and Geophysics, **35**, no. 5, 100–111.

Fomel, S., 1996, Migration and velocity analysis by velocity continuation: SEP–**92**, 159–188.

Fomel, S., 1997, Velocity continuation and the anatomy of residual prestack migration: 67th Ann. Internat. Meeting, Soc. Expl. Geophys., 1762–1765.

Fomel, S., 1998, Velocity continuation by spectral methods: SEP–**97**, 157–172.

Hale, D., 1991, Course notes: Dip moveout processing: Soc. Expl. Geophys.

Hubral, P., Tygel, M., and Schleicher, J., 1996, Seismic image waves: Geophysical Journal International, **125**, 431–442.

Kim, Y. C., Hurt, W. B., Maher, L. J., and Starich, P. J., 1997, Hybrid migration: A cost-effective 3-D depth-imaging technique: Geophysics, **62**, no. 02, 568–576.

Larner, K., and Beasley, C., 1987, Cascaded migrations—Improving the accuracy of finite-difference migration: Geophysics, **52**, no. 5, 618–643.

Rothman, D. H., Levin, S. A., and Rocca, F., 1985, Residual migration – applications and limitations: Geophysics, **50**, no. 1, 110–126.

Sava, P., 1999, Short note–on Stolt prestack residual migration: SEP–**100**, 151–158.

Schleicher, J., Hubral, P., Hocht, G., and Liptow, F., 1997, Seismic constant-velocity remigration: Geophysics, **62**, no. 02, 589–597.

Stolt, R. H., 1978, Migration by Fourier transform: Geophysics, **43**, no. 1, 23–48.

Stolt, R. H., 1996, Short note - A prestack residual time migration operator: Geophysics, **61**, no. 02, 605–607.

Toldi, J., 1985, Velocity analysis without picking: Ph.D. thesis, Stanford University.